ACS APPLIED POLYMER MATERIALS

pubs.acs.org/acsapm

Article

Utilizing Lubricant Loss from Omniphobic Coatings as a Multifunctional Delivery Mechanism

Callum Stewart,* Babak Mehrjou, Hui Huang, Yunxin Long, Kyler Chow, Tsz Wai Kok, Paul K. Chu, and Linxian Li

Cite This: *ACS Appl. Polym. Mater.* 2023, 5, 1046−1055

Read Online

ACCESS | Metrics & More | Article Recommendations | Supporting Information

ABSTRACT: Silicon-based lubricant-infused surfaces (LIS) have revolutionized the surface and interface science field with their omniphobic properties. Polydimethylsiloxane (PDMS) LIS have demonstrated excellent potential for many biological, food, or cosmetic applications. However, translation into industry faces limitations for synthesis methodologies, reagent expense, retention of omniphobicity, and legislature concerning lubricant migration. Preventing lubricant loss and retention of omniphobicity has been widely investigated, but what if the gradual lubricant depletion could be utilized for releasing active agents? Herein, we produce silicone-based organogel LIS via spontaneous 1-step polyurea reactions (Silgels) and functionalize with silver nanoparticles (Ag NP). We comparatively examined their physicochemical properties, omniphobic dewetting for probe liquids and complex mixtures (foodstuffs), and biocompatibility with mammalian and bacterial cultures. Overall, we present an easily scalable methodology to produce multifunctional, biocompatible LIS that has potential for the food packaging, cosmetic, and biological industries.

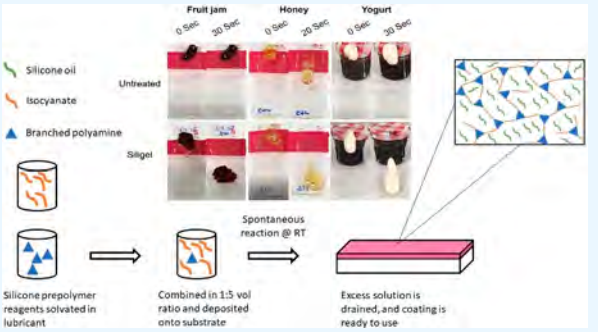

KEYWORDS: *omniphobic, polydimethylsiloxane, lubricant infused surfaces (LIS), silver nanoparticles, organogel*

1. INTRODUCTION

Slippery lubricant-infused porous surfaces (SLIPS) have revolutionized surface and interface science, finding various applications.[1] The bioinspired surfaces replicated the Pitcher Plant by initially combining specific surface topologies, low energy surface chemistries, and infused lubricants.[2,3] The newer generations of lubricant-infused surfaces (LIS) and omniphobic coatings come in a variety of approaches: surface modification with fluoridated silanes,[4] the production of long chain polymer brushes to produce a "liquid-like" effect (SOCALs),[5] fluorosilane silica or titania nanoparticle coatings,[6] and organogels of perfluoro or silicon polymers. These LIS fabrication approaches have proven to create effective omniphobic surfaces with some technologies translating into small companies, such as perfluororesins, fluorosilanes, and fluoridated NP coatings.

Research focus shifted toward the more environmentally and cost-friendly silicone materials, with many efforts directed to silicone-based SOCALs and organogels. Silsesquioxanes have also gained interest as components in organogel coatings due to the hardness of the nanocage structures.[7] To produce the organogel matrices, the silsesquioxanes are functionalized with terminal groups, such as isocyanates or acrylates, before being reacted with other polydimethylsiloxanes (PDMS) to produce the gel matrix. Likewise, isocyano and polyol silicones are combined utilizing polyurethane methodologies to produce organogel coatings, the Dow silicone elastomer two-part kit being a common approach. The silicone oil lubricants can be incorporated into the coating mixtures before deposition and thermal curing at >100 °C for multiple hours.[7−10] The silisesquinoxanes and other silicone polymer LIS organogel coatings have also utilized photoinitiated radical chain polymerization of (dimeth)acrylates[11] or epoxy rings.[8,12] Recent one-pot methods have removed the additional requirements for lubricant infusion postsynthesis and reduced fabrication time.[13] For example, Zhang et al.[14] utilized liquid PDMS lubricant in a polystyrene-based internal phase emulsion LIS (organogel), which could repel water and more complex liquids like milk, coffee, and ink. Typical requirements for these approaches include using organic solvents, thermal or multiple-day curing, or expensive reagents (silsesquioxanes), which can negatively affect the cost-benefit analysis or introduce substrate and/or process limitations.

LIS have various applications due to the versatility of their omniphobic nature, particularly in biological technologies and

Received: November 17, 2022
Accepted: December 6, 2022
Published: December 19, 2022

https://doi.org/10.1021/acsapm.2c01991
ACS Appl. Polym. Mater. 2023, 5, 1046−1055

food industries. For example, omniphobic biomedical devices have demonstrated a significant reduction in bacterial and protein biofouling and their associated medical problem[4,15,16] (e.g., thrombosis[17] and blood clotting[18]). Further applications can be found in stem cell expansion[19] as the repellent surfaces can reduce topologically induced differentiation and encourage the formation of 3D cell spheroids, which can help branch the functional mismatch between *in vivo* and *in vitro* for therapeutic agent development. Applying a compatible LIS to the food industry presents an opportunity to reduce food wastage from surface adhesions, as Yang et al.[20] demonstrated foodstuff sliding angles of <40° with OCH_3-terminated PDMS grafted to OH-plasma polymer surfaces at 120 °C. However, LIS experience lubricant loss and the subsequent loss of omniphobicity. The retention of lubricant is driven by the minimization of system energy, namely that the combination of the substrate (gel matrix or etched and chemically treated surface) and the incoming liquid results in greater system energy than the substrate and lubricant and is rejected.[21] However, lubricant is depleted from exposure to the incoming liquids, primarily through the droplet sliding mechanisms of full or partial cloaking.[2,21] When the incoming liquid contacts the LIS, the droplet can be fully enveloped by the oil layer or partially cloaked along the contacting interface, which then allows the droplet to slide across the surface oil layer, taking the small quantity of lubricant as the droplet is removed.[2] Likewise, the lubricant layer can be gradually removed via diffusion when wholly immersed in liquids for extended periods or washed with suitable solvents or surfactants, e.g., ethanol, *n*-hexane, dichloromethane, etc. The inevitable lubricant depletion can result in loss of omniphobicity and limit LIS transition into particular applications. Taking food applications as an example, the European Union recognizes the German Federal Institute for Risk Assessment (BfR) migration limitations of 10 mg/dm^2 (BfR XV) as the standard for many food contact materials. Thus, if the lubricant loss caused by sliding and diffusion at the lubricant−foodstuffs interface exceeds this value, then additional limitations are introduced for food storage applications. Many papers have investigated how to reduce the lubricant loss of LIS through complex fabrication approaches,[22] but what if the gradual loss of lubricant could be utilized instead? The release of therapeutic agents is a desirable function for many biomedical applications; thus, multifunctionalizing the gradual loss of lubricant would provide a natural vehicle for the release of such agents and make use of an unavoidable process.

This article aims to explore two ideas and build upon our previous work. We will characterize a silicone single-step coating (Siligel) for dewetting and biological behaviors and then test the incorporation and delivery potential of the Siligel using silver nanoparticles (Ag NPs) as an analogue. The Siligels will be compared to the perfluoro variation for the effects of chemical composition on dewetting, biological, and AgNP performance. Silver NPs were selected as they (i) are solid NPs and more robust than lipid NPs or other micelles and (ii) produce a distinct antibacterial/cytotoxic trend that can be directly monitored via standard cell quantification techniques and material characterization.

2. EXPERIMENTAL SECTION

Materials. Silmer NCO Di-100 (Sil-NCO) and Silmer NH C50 (Sil-NH) were provided by Siltech. PMX-200 silicone oil (Xiameter) was purchased from Xiameter. Liquid polydimethylsiloxane (PDMS) was purchased from Alfa Aeser (AA-PDMS). The FluorN1788 diisocyano perfluoropolyether (NCO-PFPE) and FluorN1017 hydroxyl perfluoro ether were purchased from Cytronix. The branched polyethylenimine (bPEI) (MW 800) was purchased from Sigma-Aldrich. Silver NPs (20−30 nm) were purchased from Nanoshel. RPMI1640, Dulbecco's Modified Eagle Medium, fetal bovine serum (FBS), and penicillin−streptomycin (PS) were purchased from Gibco. The mammalian Cell Counting Kit 8 (CCK-8) was purchased from Yeasen, the Bacterial Counting Colormetric Assay Kit (WST) was from BioVision, and the Live/Dead fluorescence kit was purchased from Invitrogen.

Synthesis. The Fluorogel and Siligel were synthesized using the 1-step process described in Stewart et al.[23] Briefly, the Silmer NCO Di-100 (Sil-NCO, Siltek) and Silmer NH C50 (Sil-NH, Siltek) were homogenized in the solvating PMX-200 silicone oil (Xiameter) at varying concentrations to produce coating mixtures with molar ratios of Sil-NH:Sil-NCO representing the degrees of cross-linking between the triamino silicone (Sil-NH) and the bi-isocyano linear silicone (Sil-NCO). The three stoichiometric ratios of NH_2:NCO investigated are 6:2 (3:1), 6:4 (3:2), and 6:6 (1:1) to determine the optimal degree of cross-linking and the related properties, such as lubricant retention. For example, to create a 6 NH_2:2 NCO ratio (2 Sil-NH:1 Sil-NCO molar ratio), 0.03 g of Sil-NH and 0.01 g of Sil-NCO were combined with 1 mL of Si oil in an Eppendorf tub. The coating mixture was pipetted on a clean glass slide to ensure complete surface coverage, allowed 20−120 s to react (proportional to the solution concentration), and recollected. The substrates were then stood on end to drain away excess material for a minimum of 1 h. Likewise, the NCO-PFPE and bPEI were combined in 1 mL of PFPE-OH lubricant at concentrations of 0.033 and 0.0044 g, respectively (1:1 stoichiometry). Silver NPs (20−30 nm NanoShel) were selected as our multifunctional active component and were incorporated into the coatings by mixing into the final coating solution. The required aliquot for the stated weight percent in the final coating solution was added into an Eppendorf tube and combined with the isocyano and polyamine components. The Fluorogel and Siligel coatings were applied as stated. Hydroxyl-terminated polydimethylsiloxane (OH-PDMS) (Alfa Aeser, USA) Siligel variant and an unlubricated version using *n*-hexane as solvent were synthesized for comparison and *in vacuo* examinations, respectively. The Siligel and Fluorogel coatings were deposited on cleaned tissue culture plates with increased exposure time to ensure uniform deposition.

X-ray Photoelectron Spectroscopy (XPS). XPS (K-alpha, Thermo Fisher Scientific, USA) with Al Kα excitation was used to determine the chemical states of elements. The spot size is a circular area with 800 μm diameter, and the pass energies (PE) for full survey spectrum and high resolution were 187.85 and 11.75 eV, respectively. The elemental composition and peak fittings were determined from the full scan spectrum and high-resolution spectrum, respectively, using the CASA XPS software.

Fourier-Transform Infrared (FTIR) Spectroscopy. Unlubricated Siligel and Fluorogel coatings were examined via micro-ATR FTIR spectroscopy by the Materials Characterization and Preparation Facility (MCPF) at the Hong Kong University of Science and Technology (HKUST). The samples were coated in a glass slide and examined with a Vertex 70 Hyperion 1000 (Bruker) FTIR spectrometer (30 μm spot size). The resulting spectra were analyzed using the "DigiLab Resolutions pro 4" software to determine the coating specific chemical groups.

Contact and Sliding Angles. The omniphobicity of Fluorogel and Siligel coatings was examined using RO water and diiodomethane (MeI). The contact angles (CAs) and sliding angles (SAs) were measured on a Krüss drop shape analyzer with a tilting stand and analyzed with the Krüss Advance analytical software. Static contact angles (5 μL) were fitted to the Young−Laplace fitting, while SAs (20 μL) were fitted to the "Ellipse (tangent −1)" function. After the measurements were taken ($n \geq 6$), the surfaces were washed in excess absolute ethanol and water to remove the surface layer of lubricant. The lubricant layer was then allowed to replenish via diffusion from the lubricant reservoir contained within the gel coating. The washing

https://doi.org/10.1021/acsapm.2c01991
ACS Appl. Polym. Mater. 2023, 5, 1046−1055

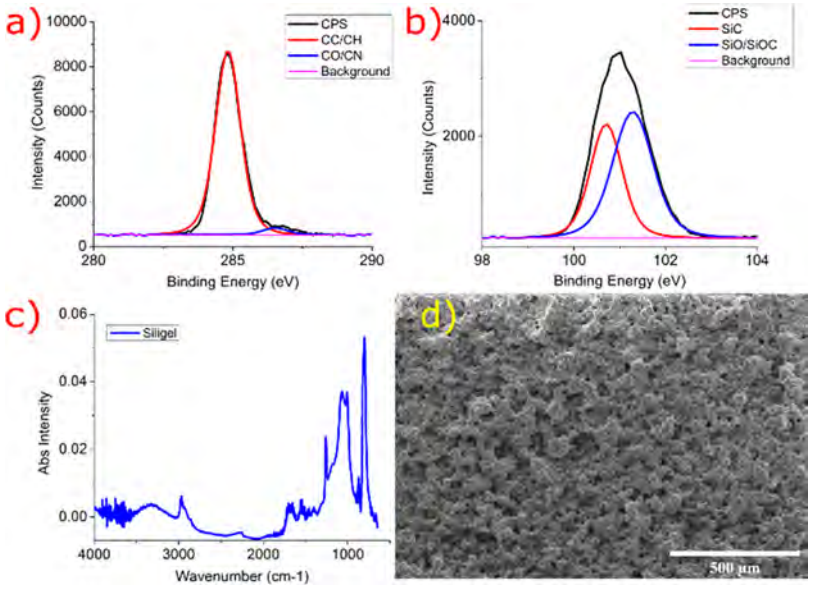

Figure 1. XPS characterization of the Siligels for Si 2p (a) and C 1s (b). (c) Full FTIR spectra from 4000 to 500 cm^{-1} for Siligel coatings (not baseline subtracted). (d) SEM of an unlubricated Siligel coating at 80× magnification. Higher resolutions resulted in surface charging, burning, and deformation.

was performed to investigate the omniphobic longevity of the coatings via accelerated lubricant loss.

Further examination of the coatings for more complex mixtures was tested on glass slides. The substrates were coated with Siligel or Fluorogel before being elevated to a fixed inclination. Four foodstuffs were examined on untreated, Siligel, and Fluorogel glass slides: fruit jam (a spatula-sized aliquot), tomato ketchup (1 mL), honey (approximately 1−2 mL), and yogurt (1 mL). Samples of the foodstuffs were transferred onto the top of the glass substrate, and the sliding time to the bottom of the glass substrate was recorded up to a maximum time of 120 s. The sliding velocity (m s^{-1}) was calculated from the distance traveled (m) and the travel time (s).

Nanoindentation. The coating toughness (Young's modulus) was measured with Piuma/Chiaro nanoindentor instruments (Optics11 life) at Sichuan University, Chengdu. The diameter of the nanoindenter was 10.5 μm, with a stiffness of 0.05 N/m and an indentation depth of 10 μm. The Young's modulus was determined by fitting the force indentation curves to known models as per the manufacturer's instructions.

Cell Culture, Proliferation Assay, and Live/Dead Fluorescence Imaging. The MDA-MB-468 breast cancer cell line and HEK-293 cell line were used for the proliferation assays and accompanying microscopy images. The cells were cultured per standard protocol[21] before seeding on 48-well plates (Corning). Briefly, the MDA and HEK cells were cultured in RPMI1640 (Gibco) medium and Dulbecco's Modified Eagle Medium (Gibco), respectively, with 10% fetal bovine serum (FBS) and 1% penicillin−streptomycin (PS). The cell lines were expanded in 6 cm Petri dishes (Corning) until 80−90% confluence. The cells were washed in phosphate buffer solution (PBS)(Gibco) and trypsinized at 37 °C and 5% CO_2 until detached. The cell suspension was spun down at 1000 rpm for 3 min and resuspended in fresh medium before seeding in the 48-well plates at 1000 and 5000 cells for MDA and HEK, respectively.

The proliferation of MDA and HEK cells was examined with the Cell Counting Kit 8 (CCK-8) (Yeasen, China) assay. The well plates were coated with the Siligel and Fluorogel coating solutions for 2 min and drained overnight before UV sterilization for 30 min. Cell proliferation was measured on days 1, 3, and 7 with 10% (v/v) CCK-8/cell media solution. The MDA and HEK cells were incubated in CCK-8 solution for 4 h alongside a blank control before transferring 100 mL aliquots to a transparent 96-well plate. The absorption was read at 450 nm using a SpectraMax M2 (Molecular Devices) plate reader.

Fluorescence imaging of the MDA and HEK cells was performed at the day 7 time point using the Invitrogen Live/Dead assay. The cells were cultured in the omniphobic coated 48-well plates as described above. The fluorescent dyes were diluted in cell medium according to the kit's instructions. Briefly, 1 mL of Calcein AM (component A) (1 vial) was transferred to the 1 μL vial of ethidium homodimer-1 (component B) to create a 2× working stock. The cell media was removed from the wells and replaced with 100 μL to cover the bottom of the well. An equal volume of working stock to cell medium (50 μL) was then transferred into the well. The cells were then incubated at room temperature for 15 min before being imaged with a (Specs fluorescence microscope and software). Green (ex/em ∼488 nm/∼515 nm) and red (ex/em ∼570 nm/∼602 nm) fluorescence filters were applied to visualize the Live/Dead cells, respectively. The exposure time for the fluorescence images was kept at 300 ms, and the gain was adjusted for optimal signal.

Bacterial Quantification Assay. The antibacterial potential for the Fluorogel and Siligel coatings was examined with the Bacterial Counting Colormetric Assay Kit (Cat# K511-500, BioVision). The electrocoupling solution (ECS) and water-soluble tetrazolium salt (WST) reagents were made up according to the instructions and stored at −20 °C until use. The *E. coli* bacteria were grown in liquid broth until an optical density (OD) of 10^9. The batch was then diluted to a 1×10^4 concentration, and 1 mL was transferred into each well of the 48-well plate. The bacteria were incubated for 3 h at 37.5 °C and then removed; the wells washed with 0.5 mL of PBS and refilled with 400 μL of 10% v/v WST/broth solution. The absorbance at 450 nm was taken initially and every subsequent 30 min. The measurements were background subtracted to account for potential Ag NPs artifact and graphed.

3. RESULTS AND DISCUSSION

Material Characterization. The Siligel and Fluorogel coatings were characterized via XPS and FTIR to determine the chemical properties. The elemental composition of the Siligel was found to be relatively constant within error across the 6:6, 6:4, and 6:2 NH_2:NCO stoichiometric coatings: 51 at. % carbon, 20 at. % oxygen, and 29% silicon with minor contributions from nitrogen. The detailed Si 2p and C 1s peaks showed the expected fittings for silicone (Figure 1a,b). The Si 2p stretches for the Siligel stoichiometries, centered around

https://doi.org/10.1021/acsapm.2c01991
ACS Appl. Polym. Mater. 2023, 5, 1046−1055

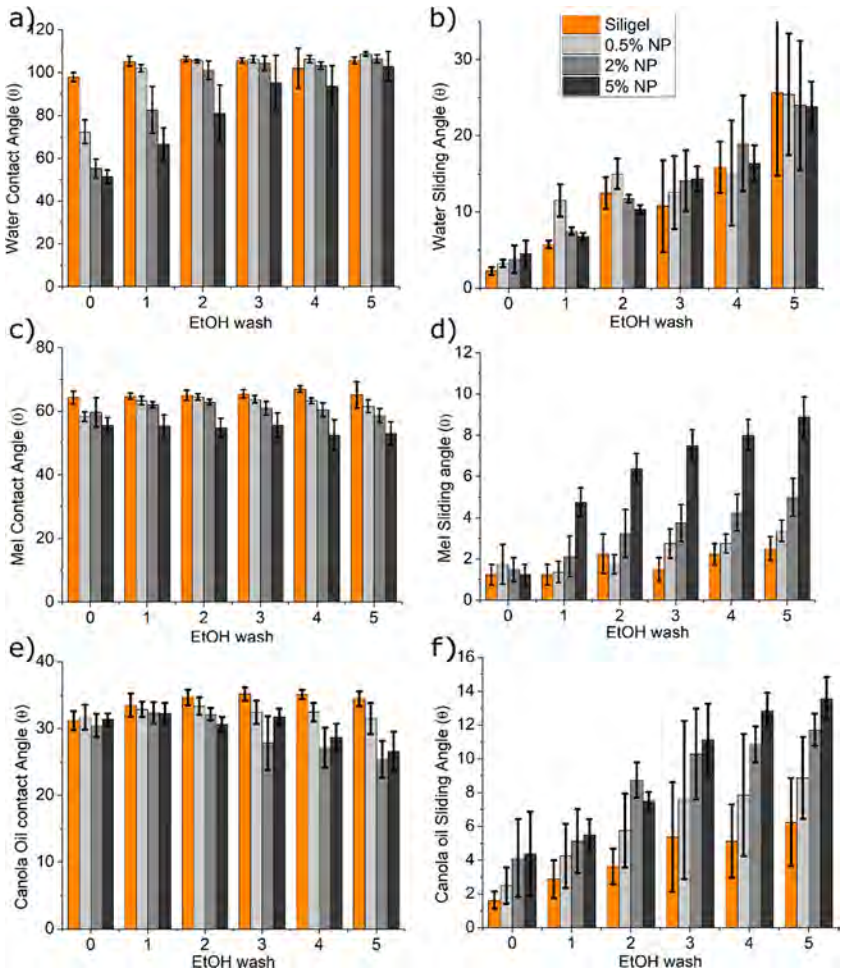

Figure 2. Contact angle (CA) and sliding angle (SA) progression for Siligel coatings with 0.5, 2, and 5 wt % Ag NP concentrations over 5× EtOH washes. The water CA shows a convergence to 100° (a) while the SA increases steadily (b) as dehydration occurs. The MeI CAs remain relatively stable with decreases over washes in proportion to AgNP concentration (c). SAs showed slight changes in the 0 and 0.5 wt % over multiple washes but drastic changes in the 2 and 5 wt % (d). Similar behavior was observed in the canola oil CAs (e) and SAs (f) with a more distinctive change in CAs and SAs according to NP wt %.

101 eV, were fitted with two curves consistent with a silicon−oxygen polymer backbone highly conjugated with CH_3 groups: Si−C at 100.8 eV and Si−O−C/Si−O at 101.4 eV.[24] The C 1s peak was centered around 285 eV, tailing off at 288 eV. The fittings agree with the known chemistry of the prepolymers, indicating the presence of abundant C−C/C−H bonds from the methyl side groups and the Sil-NCO cyclohexane groups. The CO/CN contribution originates mainly from the urea (NH-NCO) cross-linking terminals and potentially minor contributions from oxidated end terminals. The 1:1 Fluorogel agreed with the previously reported results[23] and is shown in the Supporting Information (Figure S1). Briefly, XPS showed approximately 49% F, 33% C, 15% O, and 2% N. C 1s spectra showed the typical fittings of PFPE: C−C/CH, CO/CN, and COOH peaks between 285 and 290 eV and CF_2−CF_2, CF_2−O, and O−CF_2−O in the 292−295 eV range. FTIR was also consistent with PFPE carbon and fluorine peaks.

The full spectrum scans of the Siligel-Ag NP and Fluorogel AgNP were nearly identical with their non-NP counterparts, with only a small peak indicating any presence of NP. The Ag NP- Siligels demonstrated a full spectrum scan composition of 41% C, 28.6% O, 28.3% Si, 1.85% N, and 0.25% Ag. The C 1s peaks aligned with the nonfunctionalized Siligel with a dominating C−H/C−C bond and minor contributions from the C−N/C−O. The Si2P high-resolution peaks were similar to the nonfunctionalized Siligel, centering on the 102.2 eV Si−C−O/Si−O bonds with minor contributions from the 101.2 eV Si−C groups and potentially negligible signal from the SiO_2. The elemental composition of the Ag NP-Fluorogels was determined to be approximately 43.3% C, 34.78% F, 15.96% O, 5.69% N, and 0.27% Ag. The high-resolution spectra of the Fluorogels showed the previously obtained C 1s fittings for our coatings and general perfluoro polyether: 36.15% CC/CH, 24.06% CO/CN, 5.27% CO/O−C═O, 25.28% CF2−O, and 9.24% O−CF2−O. The lack of significant distinction between the Ag NP coatings and their respective non-NP coatings can potentially be attributed to the nonuniform distribution of NPs and the XPS penetrating the top few nanometers.

FTIR analysis was performed on the Siligel (Figure 1c) and Fluorogel (Figure S1) coatings. The Siligel coatings from 500 to 4000 cm^{-1} demonstrated a series of strong peaks. The sharp peak around 3000−2850 cm^{-1} is associated with symmetric and asymmetric CH stretches, such as those found in the conjugated cyclocarbon structures of Sil-NCO. The peaks at 1800−1650 cm^{-1} can be associated with ester and amide C═O bonds, which, in conjunction with the sharp C−O peak at 1250 cm^{-1} of an alkyl aryl ether, indicates that the urea cross-linking reaction has occurred.[25] The strong peak from 1150 to

https://doi.org/10.1021/acsapm.2c01991
ACS Appl. Polym. Mater. 2023, 5, 1046−1055

1050 cm^{-1} can be assigned to C−O bonds from an aliphatic ether or secondary alcohols, while the peaks at lower wavenumbers can be attributed to the numerous CH_3 groups in the chemical structures. Overall, the physicochemical properties of the Siligel coatings fit the expectations derived from the silicone precursors. The Sil-NCO and Sil-NH reagents are silicon backbones with CH_3 groups and isocyanate or amine functional ends, respectively. The FTIR and XPS show little chemical difference between the various ratios; therefore, the contact and sliding angles must be examined to determine the optimal conditions.

The 6:6, 6:4, and 6:2 stoichiometric Siligels were probed with water, diiodomethane (MeI), and canola oil to determine if the varying degree of cross-linking produced differences in static contact angles and sliding capacities. Static contact angles (5 μL) for the Siligel were consistent in CAs across the stoichiometries: water CA approximately 100°, canola CA approximately 30−35°, and MeI around 60°.[9,14] Therefore, the sliding angles (SAs) for the three probe liquids were examined to determine the optimal coating stoichiometries and concentrations.

The 6:6, 6:4, and 6:2 stoichiometries were synthesized at three Sil-NH solution concentrations combined with the equivalent Sil-NCO concentrations, producing three corresponding thickness coatings. The deposition procedure was kept constant to ensure the coating properties were solely determined by the chemical compositions of the coating solutions. Upon visible inspection, the 0.06 g/mL Sil-NH concentrations of all three stoichiometries produced thick gel coatings, while the 0.015 g/mL Sil-NH solutions produced thin coatings—both of which resulted in sharp WSA increases from 3° to 5° to >20° by wash 1 and >30−40° by wash 2. The 0.03 g/mL Sil-NH concentrations produced a more gradual but similar behavior as previous conditions for the 6:6 and 6:4 concentrations. The 6:2 stoichiometry, however, demonstrated the best omniphobic performance by retaining WSA < 20° after 4−5 pure EtOH washes and thus was used as the standard coating formulation. The MeI CAs for the 6:2 coatings remained around 62° (Figure 2c) while the sliding angle remained below 3−4° inclination across all washes (Figure 2d). The canola oil CAs increased slightly from 32° to 35° (Figure 2.e) while the SAs increased from approximately 1.5° to around 6° after 5× washes. The inclusion of Ag NPs into the Siligel coatings demonstrated a weight percent correlated trend in wetting properties. The water contact angles (WCAs) demonstrate a lubricant loss/hydrophobic recovery trend over the first 3 EtOH washes (Figure 1a). The 0.5 wt % coatings increased from 72° to 102° after 1 wash, the 2 wt % increased from 55° to 101° after 2 washes, and finally 51° to 95° over three washes for the 5 wt % coatings.

All Ag NP coatings started at 1−2° water SAs before steadily increasing to 25 ± 10° inclination, with minor contributions from NP wt % (Figure 2b). The MeI CAs were consistent across all washes, with the 5 wt % coatings having lower CAs (approximately 55°) than the 0.5 and 2 wt % (approximately 60°) (Figure 2c). The SAs for MeI do not show as much sensitivity to the dehydration/washes with increases from 1° to 2.5° for non-Ag NP coatings and 1.8° to 3.4° on the 0.5 wt %, but the 2 and 5 wt % demonstrated considerably greater changes, from 1.5° to 5° and 1.3° to 8.9°, respectively. The effect of NP wt %, and by extension surface roughness, was further demonstrated with the canola oil. The CAs were largely homogeneous up to wash 3, but the 2 and 5 wt % started reducing CA compared to the non-NP Siligel, decreasing from 32° to around 25°. The SAs were found to increase in steps proportional to the wt %; the non-NP Siligel increased from 1.5° to 6°, 0.5 wt % from 2.5° to 8.9°, the 2 wt % from 4.1° to 11.7°, and the 5 wt % from 4.4° to 13.6°. The wetting properties of the Siligels were further examined by replacing the Xiameter Si oil with an OH-terminated PDMS (Alfa Aeser) (AA-PDMS). The AA-PDMS lubricated Siligels demonstrated highly similar water and MeI contact angle to the Xiameter Siligel. The WCAs increased from 90° at 0× wash to 110° at 1× wash onward, while the MeI CAs remained constant around 60°. The water SAs for the AA-PDMS started at 1−2° inclination with excess oil at the surface but increased to 30 ± 10° from 1× wash. The MeI SA, however, increased from 1° to 4° over the 5× washes, as is consistent with the Xiameter Siligels. The PDMS Siligel graphs and images of the water and MeI droplets used for contact and sliding angle measurements can be found in the Supporting Information.

Ag NPs in Fluorogels also produced changes to the contact and sliding angles. The WCA for nonfunctionalized Fluorogels started at ∼50° and increased to 75−80° by 3× washes, while the 0.5, 2, and 5 wt % had initial WCAs of 40°, 34°, and 30°, respectively, and stabilized between 70° and 80° after 1−2 EtOH washes. The MeI CAs of the nonfunctionalized Fluorogel started at approximately 70° and gradually increase to 80° over the 5 EtOH washes, whereas the NP-functionalized coatings had initial CAs between 58 and 65 and stabilized at 70° after 1 wash. The water and MeI SAs of the standard Fluorogel remained below 5° (Figure S3), while the Ag NP functionalized coatings demonstrated a gradual increase from 2° to 5° to approximately 15°. The MeI SAs for the NP coatings remained below 5° but demonstrated a similar trend to the Siligel, with the SAs increasing proportionally to the NP concentration.

The complex liquids of honey, tomato ketchup, yogurt, and jam were used to further probe the omniphobic properties of the Fluorogel and Siligel coatings and further explore their capacity for food storage. Tomato ketchup, fruit jam, honey, and yogurt were selected as they are complex mixtures and are representative of the more viscous foodstuffs that experience noticeable adhesion to packaging. Glass slides were coated with Siligel and Fluorogel before the described quantities of ketchup, honey, and fruit jam were deposited at the top of the slides and allowed to migrate smoothly and continuously down the surface under the influence of gravity. The inclination angle of yogurt was increased to 39°, and the process was repeated. The sliding velocities for the foodstuffs are shown in Table 1.

Table 1. Foodstuff Sliding Velocities (m s^{-1}) on Uncoated and Fluorogel and Siligel Coated Glass Slides

	fruit jam	honey	ketchup	yogurt
uncoated	0	0.0013	0.00025	0.00027
Fluorogel	0.00067	0.0013	0.0005	0.00078
Siligel	0.0014	0.0030	0.001	0.0018

The results for each foodstuff examined demonstrated that the Siligel coatings possessed better sliding velocities than the uncoated and Fluorogel coated glass slides. Furthermore, the foodstuffs aliquots were less spread and left behind less residue on the Siligel coatings compared to the Fluorogel coated and uncoated glass control (Figure 3). For comparison, Yang et al.[20] demonstrated foodstuff sliding angles of <40° with OCH_3-

https://doi.org/10.1021/acsapm.2c01991
ACS Appl. Polym. Mater. 2023, 5, 1046−1055

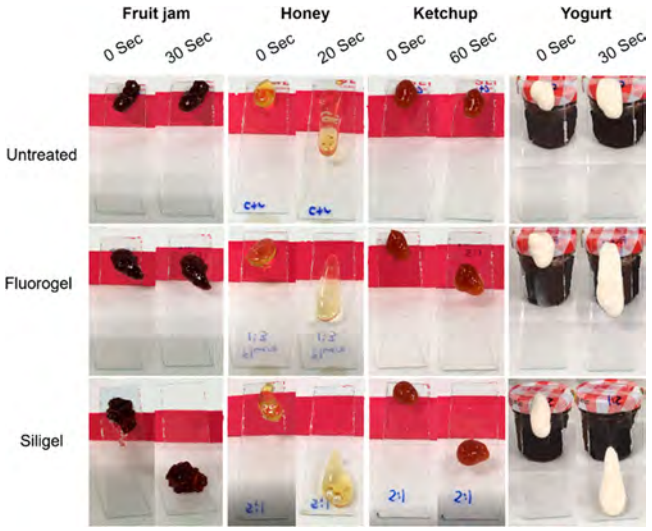

Figure 3. Sliding of various condiments and dairy products on untreated, Fluorogel, and Siligel coated glass slides. The inclination angle for jam, honey, and ketchup were approximately 25° elevation, while the yogurt was approximately 39°. The sliding behavior showed some variation based on the foodstuff; however, the Siligel consistently had the highest rate of sliding and the lowest amount of remaining material once sliding was completed.

terminated PDMS grafted to OH-plasma polymer surfaces at 120 °C. Our Siligel coatings produced sliding angles of approximately 25° for sauces, jam, and honey and 40° for yogurt with a fraction of the processing time and equipment. Overall, the combination of the clean and quick sliding and the rapid, simple fabrication methodology strongly suggests that the Siligel coatings have strong potential applications in the food processing, storage, and transportation markets.

Table 2. Foodstuff Sliding Velocities (m s^{-1}) on Uncoated and Fluorogel and Siligel Coated Glass Slides

	fruit jam	honey	ketchup	yogurt
uncoated	0	0.0013	0.00025	0.00027
Fluorogel	0.00067	0.0013	0.0005	0.00078
Siligel	0.0014	0.0030	0.001	0.0018

While the Siligel and Fluorogel coatings demonstrated good omniphobicity toward both simple and complex water and oil-based liquids, the mechanical testing demonstrated soft but flexible coatings. Nanoindentation performed on lubricated and unlubricated Siligels at Sichuan University showed a considerable reduction in modulus compared to the steel sheet substrate. The modulus for the uncoated steel substrate (1840 ± 263 kPa) was 10× larger than the unlubricated Siligels (130−200 kPa), which in turn were 30× larger than the lubricated coatings (4−8 kPa). No significant differences were found between the varying NP concentrations. While mechanical durability is a reoccurring problem for omniphobic organogels, potential avenues for improving the toughness include incorporating additional elements, e.g., nanoclay particles,[26] or substituting the isocyano/polyamine polymer.[27] Despite the mechanical limitations to nonabrasive applications, our polyurea coatings provide a more industry-friendly approach by (i) homogenizing the isocyano and polyamine polymers in their respective lubricants, removing the need for organic solvents and infusion steps, (ii) utilizing a spontaneous reaction at room temperature and eliminating the need for and substrate restrictions of thermal curing or photocuring, and (iii) utilizing reagents that are nonvolatile, inexpensive, and available in manufacturing quantities, thereby reducing potential hazards and costs.

Mammalian and Bacterial Cell Assays. The cell establishment, proliferation, and spreading behaviors of MDA-MB-468 and HEK-293 cell lines were used to evaluate the potential of the Fluorogels and Siligels for biointerfaces and medical devices. The proliferation of the cells on the standard and Ag NP incorporated coatings was measured via CCK-8 assay and contrast microscopy at days 1, 3, and 7 postseeding (Figure 4a−d). Both omniphobic coatings demonstrate cellular proliferation capacity with a lower establishment potential than the TCP control, usually ranging between 1/3 and 2/3 of the TCP signal. There was a significant variation within the measured absorptions of the non-AgNP coatings ($n \geq 12$) and between sets, believed to result from unavoidable external factors and cell passage variability. Despite these factors, the Ag NP coatings demonstrated a consistent, albeit cytotoxic, signal across the coatings and cell lines with no measurable signal over the baseline. Contrast microscopy images were taken on a Nikon Eclipse Ts2 light microscope to visualize the growth and spreading behavior of the MDA and HEK cells at days 1, 3, and 7. Untreated TCP wells had the standard 2D cell spreading cumulating in multilayers by day 7, while the non-Ag NP Siligel had localized regions of 2D cell growth. The cells on Ag-NP Fluorogel and Siligel coatings were rounded and largely removed during handling, with the few that remained on individual wells accounting for the slightly elevated signals in the Siligel-MDA (Figure 4a) and Fluorogel-MDA (Figure 4b) graphs. The non-Ag NP Fluorogel, however, demonstrated the ability to produce 3D cell spheroids by day 7 without any additional media reagents (Figure S5).

Fluorescent Live/Dead imaging, performed at the day 7 time point, confirmed the growth behaviors of the MDA and HEK cells on the coatings. The 0 wt % Siligel coatings demonstrated regions of a healthy "live" cell culture for the HEK and MDA cell lines, as shown by the abundant green signal in Figure 5. In contrast, the 2 wt % Ag coatings largely prevent cell establishment and produced isolated weak dead "red" signals. Similar behaviors were observed in the Fluorogels (Figure S5).

The *E. coli* demonstrated similar trends to the mammalian cell proliferation assays. Initial testing procedures produced a large absorbance across all Ag NP-Siligel conditions <2 wt %, while minimal signal was observed across all Ag NP-Fluorogel conditions. To eliminate the detection of free-floating resulting from the omniphobic coatings rather than attached bacteria, the initial bacterial broth was removed and then replaced with 10% WST/LB solution. The signal intensity was reduced by approximately 4−5 times across all conditions with the Ag NP Siligel coatings demonstrating a nearly complete bactericidal effect. The TCP results demonstrated specific signals of 0.33 ± 0.04 and 0.23 ± 0.06, while the nonfunctionalized omniphobic coatings showed specific signals of 0.22 ± 0.07 and 0.10 ± 0.03 for the Fluorogel and Siligel, respectively. The inclusion of final 0.2 wt % Ag NPs and above in the Fluorogel and Siligel rendered the coatings antibacterial. The WST bacterial proliferation assay suggests a potential difference in the interactions between the included Ag NPs and the omniphobic coating, Fluorogel, or Siligel. Antibacterial action, indicated by baseline WST signal, was observed across all Fluorogel AgNP concentrations in both variations of the assays (with and

https://doi.org/10.1021/acsapm.2c01991
ACS Appl. Polym. Mater. 2023, 5, 1046−1055

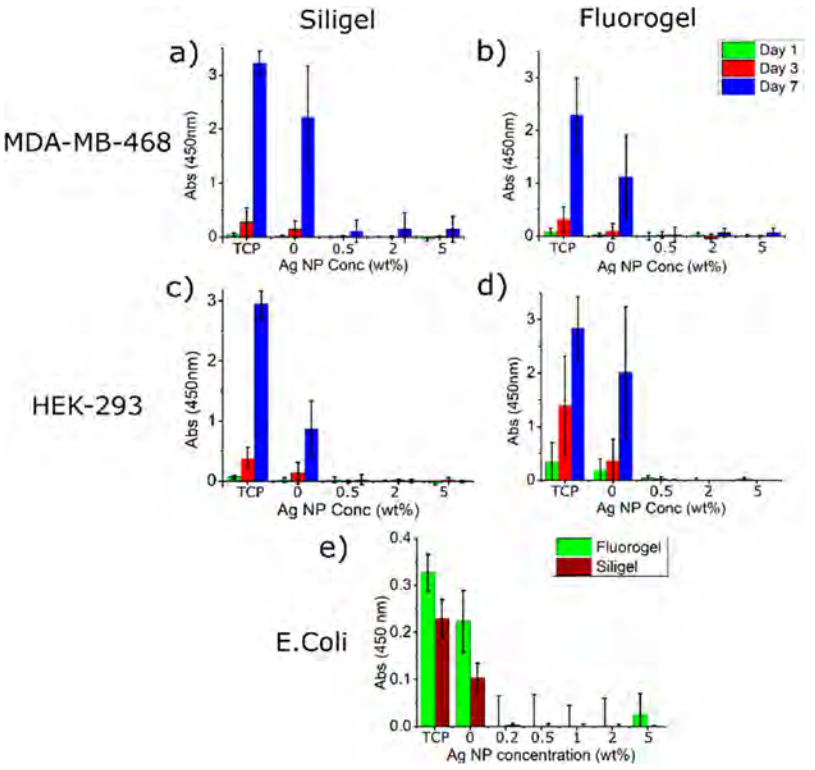

Figure 4. CCK-8 absorbance (450 nm) for MDA on Siligel (a), Fluorogel (b), HEK Siligel (c), and Fluorogel (d) at the given Ag NP wt % of the coating solution. The results show a relatively universal trend of equivalent or reduced cell proliferation of the non-Ag NP coatings while near complete cell apoptosis was observed from 0.5 wt % upward. In addition, *E. coli* growth on the Fluorogel and Siligel coatings (e) with increasing Ag NP concentrations shows the same immediate drop in bacterial signal as the mammalian assays.

without LB replacement), indicating that the Ag NPs have the potential to migrate out of the coatings into the liquid broth solution. The NP-Siligel demonstrated antibacterial functioning at 2 wt % or above according to the "without LB removal" assay conditions, but the near-baseline signal across all concentrations after the liquid broth was replaced, suggesting the Ag NPs did not as readily migrate from the Siligel coatings. The differences in migration could be attributed to chemical and physical interactions. The Fluorogel contains polar perfluoropolymers as gel components and lubricants, which can interact with the Ag NPs through surface charges. Conversely, the chemically inert, nonpolar silicones do not. Additionally, the physical polymer matrix of the Fluorogel consists of a branched PEI (6× NH_2, 800 g mol^{-1}) and perfluoropolyether (2× NCO, 2000 g mol^{-1}), while the Siligel is composed of a branched amine (3× NH_2, 116000 g mol^{-1}) and linear isocyanate (2× NCO, 8000 g mol^{-1}). The differences in branched polyamine coordinations and dendrite structure result in different pore structures, which would influence the capacity of NPs and lubricant to migrate through the polymer. Overall, the Ag NP functionalized coatings demonstrated considerable antibacterial activity and highlighted the potential for multifunctional omniphobic coatings.

The addition of omniphobicity to biomedical devices has demonstrated a significant reduction in bacterial and protein attachment,[4,15,28] thus reducing the problems of bacterial and fungal biofilm formation. However, the LIS benefits rely on the lubricant, which is lost over time through lubricant−liquid sliding interactions. Rather than attempting to prevent lubricant dehydration, we demonstrated that the inevitable process can in utilized to deliver a payload in the form of Ag NPs, as shown by the *in vitro* assays at 0.2 wt % compared to previous concentrations of 1 wt %.[13] Other antibacterial reagents that could be incorporated into omniphobic LIS include crystal violet[29] antithrombotic agents, functional lipid NPs, or more organic reagents such as black seed oil[30] or natural antimicrobial oils (carvacrol, thymol, cinnamaldehyde, etc.). Therefore, the multifunctionalization of omniphobic coatings represents a novel avenue for investigation which can utilize pre-existing knowledge from hydrogel and other therapeutic release materials to create tailorable omniphobic organogel coatings.

4. CONCLUSION

Silicon-based LIS have become popular in surface science thanks to their low surface energies, environmental compatibilities, and lower costs. However, the various approaches of LIS modification introduce processing limitations, and the lubricant loss inherent to LIS introduces legal regulation complications. Herein, we synthesized a 1-step multifunctionalized silicone LIS based on our previous polyurea method. XPS and FTIR demonstrate spectra consistent with other silicone coatings while the sliding potential was reduced proportionally to the NP wt %. The nonfunctionalized coatings showed mammalian and bacterial growth, with Fluorogels producing 3D cell cultures, while antibacterial and cytotoxic behavior was observed from 0.2 wt % Ag NP concentrations. Overall, the Fluorogels and Siligels allow their application in numerous non- or low-contacting omniphobic applications (foodstuff storage, cell culture expansion, biomedical devices, etc.) while providing a versatile platform for further investigation into multifunctional LIS.

https://doi.org/10.1021/acsapm.2c01991
ACS Appl. Polym. Mater. 2023, 5, 1046−1055

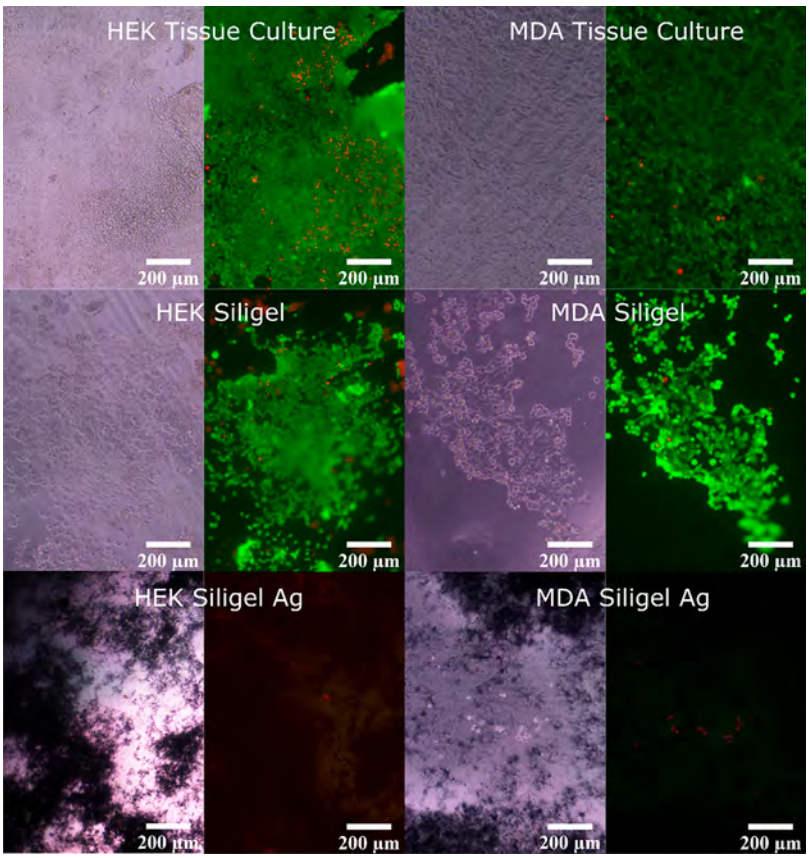

Figure 5. Contrast and Live/Dead fluorescence microscopy images of the MDA-MB and HEK permanent cell lines at 10× magnification after 7 days on TCP and Siligel coatings at 0 and 2 wt % AgNP.

■ ASSOCIATED CONTENT

Supporting Information

The Supporting Information is available free of charge at https://pubs.acs.org/doi/10.1021/acsapm.2c01991.

Figure S1: XPS fittings for C 1s and Si 2p spectra of Sil_NCO and Sil-NH; Figure S2: sliding and contact angles for the Silmer NCO Di-50 (Sil-NCO) and Silmer NH C50 (Sil-NH) deposited on glass substrates; Figure S3: contact and sliding measurements of MeI and water on the 0 and 5 wt % Ag NP Siligel coatings; Figure S4: wetting measurements for Fluorogels at increasing Ag NP wt %; (a) water contact angle, (b) water sliding angle, (c) MeI contact angle, and (d) MeI sliding angle; Table S1: sliding distance and time for foodstuffs on untreated, Fluorogel, and Siligel surfaces; Figure S5: contrast and Live/Dead fluorescence microscopy images of the MDA-MB and HEK permanent cell lines at 10× magnification after 7 days on TCP and Fluorogel coatings at 0 and 2 wt % AgNP (PDF)

■ AUTHOR INFORMATION

Corresponding Author

Callum Stewart − *Karolinska Institutet Ming Wai Lau Centre for Reparative Medicine, 999077 Sha Tin, Hong Kong;* orcid.org/0000-0001-9474-4358; Email: callum.stewart@ki.se

Authors

Babak Mehrjou − *Department of Materials Science and Engineering, Department of Physics and Department of Biomedical Engineering, City University of Hong Kong, 999077 Kowloon Tong, Hong Kong;* orcid.org/0000-0003-3493-6598

Hui Huang − *Karolinska Institutet Ming Wai Lau Centre for Reparative Medicine, 999077 Sha Tin, Hong Kong*

Yunxin Long − *Karolinska Institutet Ming Wai Lau Centre for Reparative Medicine, 999077 Sha Tin, Hong Kong*

Kyler Chow − *Karolinska Institutet Ming Wai Lau Centre for Reparative Medicine, 999077 Sha Tin, Hong Kong*

Tsz Wai Kok − *Developmental and Regenerative Biology TRP, School of Biomedical Sciences, Faculty of Medicine, The Chinese University of Hong Kong, 518172 Ma Liu Shui, Hong Kong*

Paul K. Chu − *Department of Materials Science and Engineering, Department of Physics and Department of Biomedical Engineering, City University of Hong Kong, 999077 Kowloon Tong, Hong Kong;* orcid.org/0000-0002-5581-4883

Linxian Li − *Karolinska Institutet Ming Wai Lau Centre for Reparative Medicine, 999077 Sha Tin, Hong Kong*

Complete contact information is available at: https://pubs.acs.org/10.1021/acsapm.2c01991

Notes

The authors declare no competing financial interest.

■ ACKNOWLEDGMENTS

Funding was provided by the Karolinska Institutet internal fund, Ming Wai Lau Centre grant.

REFERENCES

(1) Mackie, G.; Gao, L.; Yau, S.; Leslie, D. C.; Waterhouse, A. Clinical Potential of Immobilized Liquid Interfaces: Perspectives on Biological Interactions. *Trends Biotechnol.* **2019**, *37* (3), 268−280.

(2) Villegas, M.; Zhang, Y.; Abu Jarad, N.; Soleymani, L.; Didar, T. F. Liquid-Infused Surfaces: A Review of Theory, Design, and Applications. *ACS Nano* **2019**, *13* (8), 8517−8536.

(3) Yong, J.; Chen, F.; Yang, Q.; Fang, Y.; Huo, J.; Zhang, J.; Hou, X. J. A. M. I. Nepenthes inspired design of self-repairing omniphobic slippery liquid infused porous surface (SLIPS) by femtosecond laser direct writing. *Adv. Mater. Interfaces.* **2017**, *4* (20), 1700552.

(4) Yin, J.; Mei, M. L.; Li, Q.; Xia, R.; Zhang, Z.; Chu, C. H. Self-cleaning and antibiofouling enamel surface by slippery liquid-infused technique. *Sci. Rep.* **2016**, *6* (1), 25924.

(5) Wang, L.; McCarthy, T. J. Covalently Attached Liquids: Instant Omniphobic Surfaces with Unprecedented Repellency. *Angew. Chem., Int. Ed.* **2016**, *55* (1), 244−248. Cheng, D. F.; Masheder, B.; Urata, C.; Hozumi, A. Smooth Perfluorinated Surfaces with Different Chemical and Physical Natures: Their Unusual Dynamic Dewetting Behavior toward Polar and Nonpolar Liquids. *Langmuir* **2013**, *29* (36), 11322−11329.

(6) Lu, Y.; He, G.; Carmalt, C. J.; Parkin, I. P. Synthesis and characterization of omniphobic surfaces with thermal, mechanical and chemical stability. *RSC Adv.* **2016**, *6* (108), 106491−106499. Sun, Y.; Guo, Z. Novel and cutting-edge applications for a solvent-responsive superoleophobic-superhydrophilic surface: Water-infused omniphobic surface and separating organic liquid mixtures. *Chem. Eng. J.* **2020**, *381*, 122629. Li, X.; Shan, H.; Cao, M.; Li, B. Facile fabrication of omniphobic PVDF composite membrane via a waterborne coating for anti-wetting and anti-fouling membrane distillation. *J. Membr. Sci.* **2019**, *589*, 117262.

(7) Zhang, K.; Huang, S.; Wang, J.; Liu, G. Transparent organic/silica nanocomposite coating that is flexible, omniphobic, and harder than a 9H pencil. *Chem. Eng. J.* **2020**, *396*, 125211.

(8) Zhang, K.; Huang, S.; Wang, J.; Liu, G. Transparent Omniphobic Coating with Glass-Like Wear Resistance and Polymer-Like Bendability. *Angew. Chem., Int. Ed. Engl.* **2019**, *58* (35), 12004−12009.

(9) Hu, H.; Wang, J.; Wang, Y.; Gee, E.; Liu, G. Silicone-Infused Antismudge Nanocoatings. *ACS Appl. Mater. Interfaces* **2017**, *9* (10), 9029−9037.

(10) Gee, E.; Liu, G.; Hu, H.; Wang, J. Effect of Varying Chain Length and Content of Poly(dimethylsiloxane) on Dynamic Dewetting Performance of NP-GLIDE Polyurethane Coatings. *Langmuir* **2018**, *34* (34), 10102−10113.

(11) Yao, X.; Dunn, S. S.; Kim, P.; Duffy, M.; Alvarenga, J.; Aizenberg, J. Fluorogel Elastomers with Tunable Transparency, Elasticity, Shape-Memory, and Antifouling Properties. *Angew. Chem., Int. Ed.* **2014**, *53* (17), 4418−4422. Zheng, C.; Liu, G.; Hu, H. UV-Curable Antismudge Coatings. *ACS Appl. Mater. Interfaces* **2017**, *9* (30), 25623−25630.

(12) Bender, D. N.; Zhang, K.; Wang, J.; Liu, G. Hard yet Flexible Transparent Omniphobic GPOSS Coatings Modified with Perfluorinated Agents. *ACS Appl. Mater. Interfaces* **2021**, *13* (8), 10467−10479.

(13) Wang, K.; He, J. One-Pot Fabrication of Antireflective/Antibacterial Dual-Function Ag NP-Containing Mesoporous Silica Thin Films. *ACS Appl. Mater. Interfaces* **2018**, *10* (13), 11189−11196.

(14) Zhang, D.; Xia, Y.; Chen, X.; Shi, S.; Lei, L. PDMS-Infused Poly(High Internal Phase Emulsion) Templates for the Construction of Slippery Liquid-Infused Porous Surfaces with Self-cleaning and Self-repairing Properties. *Langmuir* **2019**, *35* (25), 8276−8284.

(15) Yuan, S.; Luan, S.; Yan, S.; Shi, H.; Yin, J. Facile Fabrication of Lubricant-Infused Wrinkling Surface for Preventing Thrombus Formation and Infection. *ACS Appl. Mater. Interfaces* **2015**, *7* (34), 19466−19473.

(16) Waterhouse, A.; Leslie, D.; Lightbown, K.; Antonoff, D.; Lightbown, S.; Dimitrakakis, N.; Hicks-Berthet, J.; Leslie, C.; Super, M.; Ingber, D.; Ackerman, M. Rapid Coating Process Generates Omniphobic Dentures in Minutes to Reduce C. albicans Biofouling. *ACS Biomater. Sci. Eng.* **2019**, *5* (2), 420−424.

(17) Leslie, D. C; Waterhouse, A.; Berthet, J. B; Valentin, T. M; Watters, A. L; Jain, A.; Kim, P.; Hatton, B. D; Nedder, A.; Donovan, K.; Super, E. H; Howell, C.; Johnson, C. P; Vu, T. L; Bolgen, D. E; Rifai, S.; Hansen, A. R; Aizenberg, M.; Super, M.; Aizenberg, J.; Ingber, D. E A bioinspired omniphobic surface coating on medical devices prevents thrombosis and biofouling. *Nat. Biotechnol.* **2014**, *32* (11), 1134−1140.

(18) MacCallum, N.; Howell, C.; Kim, P.; Sun, D.; Friedlander, R.; Ranisau, J.; Ahanotu, O.; Lin, J. J.; Vena, A.; Hatton, B.; Wong, T.-S.; Aizenberg, J. Liquid-Infused Silicone As a Biofouling-Free Medical Material. *ACS Biomater. Sci. Eng.* **2015**, *1* (1), 43−51. Roberts, T. R.; Leslie, D. C.; Cap, A. P.; Cancio, L. C.; Batchinsky, A. I. Tethered-liquid omniphobic surface coating reduces surface thrombogenicity, delays clot formation and decreases clot strength ex vivo. *Biomed. Mater. Res. B Appl. Biomater.* **2020**, *108* (2), 496−502.

(19) Jellali, R.; Paullier, P.; Fleury, M.-J.; Leclerc, E. Liver and kidney cells cultures in a new perfluoropolyether biochip. *Sens. Actuators, B* **2016**, *229*, 396−407.

(20) Yang, C.; Wu, Q.; Zhong, L.; Lyu, C.; He, G.; Yang, C.; Li, X.; Huang, X.; Hu, N.; Chen, M.; Hang, T.; Xie, X. Liquid-like polymer-based self-cleaning coating for effective prevention of liquid foods contaminations. *J. Colloid Interface Sci.* **2021**, *589*, 327−335.

(21) McHale, G.; Afify, N.; Armstrong, S.; Wells, G. G.; Ledesma-Aguilar, R. The Liquid Young's Law on SLIPS: Liquid-Liquid Interfacial Tensions and Zisman Plots. *Langmuir* **2022**, *38* (32), 10032−10042.

(22) Howell, C.; Vu, T. L.; Lin, J. J.; Kolle, S.; Juthani, N.; Watson, E.; Weaver, J. C.; Alvarenga, J.; Aizenberg, J. Self-Replenishing Vascularized Fouling-Release Surfaces. *ACS Appl. Mater. Interfaces* **2014**, *6* (15), 13299−13307. Huang, S.; Liu, G.; Hu, H.; Wang, J.; Zhang, K.; Buddingh, J. J. C. E. J. Water-based anti-smudge NP-GLIDE polyurethane coatings. *Chem. Eng. J.* **2018**, *351*, 210−220. Baumli, P.; D'Acunzi, M.; Hegner, K. I.; Naga, A.; Wong, W. S. Y.; Butt, H.-J.; Vollmer, D. The challenge of lubricant-replenishment on lubricant-impregnated surfaces. *Adv. Colloid Interface Sci.* **2021**, *287*, 102329. Hu, H.; Liu, G.; Wang, J. Preparation and comparison of NP-GLIDE, SLIPS, superhydrophobic, and other coatings from identical precursors at different mixing ratios. *J. Mater. Chem. A* **2019**, *7* (4), 1519−1528.

(23) Stewart, C. A. C.; Kok, T. W.; Lee, K. H. K.; Li, L. A spontaneous one-step fabrication of slippery gel coatings. *Appl. Surf. Sci.* **2022**, *572*, 151341.

(24) Kaur, A.; Chahal, P.; Hogan, T. J. I. E. D. L. Selective fabrication of SiC/Si diodes by excimer laser under ambient conditions. *IEEE Electron Device Lett.* **2016**, *37* (2), 142−145.

(25) Cui, J.; Daniel, D.; Grinthal, A.; Lin, K.; Aizenberg, J. Dynamic polymer systems with self-regulated secretion for the control of surface properties and material healing. *Nat. Mater.* **2015**, *14*, 790.

(26) Fogelström, L.; Malmström, E.; Johansson, M.; Hult, A. Hard and Flexible Nanocomposite Coatings using Nanoclay-Filled Hyperbranched Polymers. *ACS Appl. Mater. Interfaces* **2010**, *2* (6), 1679−1684.

(27) Gao, P.; Wang, Y.; Wang, J.; Wang, F.; Ma, W.; Zhang, Z.; Men, X.; Lu, Y. Rational Design of Durable Anti-fouling Coatings with High Transparency, Hardness, and Flexibility. *ACS Appl. Mater. Interfaces* **2022**, *14* (25), 29156−29166.

(28) Kratochvil, M. J.; Welsh, M. A.; Manna, U.; Ortiz, B. J.; Blackwell, H. E.; Lynn, D. M. Slippery Liquid-Infused Porous Surfaces that Prevent Bacterial Surface Fouling and Inhibit Virulence Phenotypes in Surrounding Planktonic Cells. *ACS Infect. Dis.* **2016**, *2* (7), 509−517. Chen, J.; Howell, C.; Haller, C. A.; Patel, M. S.; Ayala, P.; Moravec, K. A.; Dai, E.; Liu, L.; Sotiri, I.; Aizenberg, M.; Aizenberg, J.; Chaikof, E. L. An immobilized liquid interface prevents device associated bacterial infection in vivo. *Biomaterials* **2017**, *113*, 80−92.

(29) Patir, A.; Hwang, G. B.; Lourenco, C.; Nair, S. P.; Carmalt, C. J.; Parkin, I. P. Crystal Violet-Impregnated Slippery Surface to Prevent

https://doi.org/10.1021/acsapm.2c01991
ACS Appl. Polym. Mater. 2023, 5, 1046−1055

Bacterial Contamination of Surfaces. *ACS Appl. Mater. Interfaces* **2021**, *13* (4), 5478−5485.
(30) Habib, S.; Zavahir, S.; Abusrafa, A. E.; Abdulkareem, A.; Sobolčiak, P.; Lehocky, M.; Vesela, D.; Humpolíček, P.; Popelka, A. Slippery Liquid-Infused Porous Polymeric Surfaces Based on Natural Oil with Antimicrobial Effect. *Polymers* **2021**, *13* (2), 206.

https://doi.org/10.1021/acsapm.2c01991
ACS Appl. Polym. Mater. 2023, 5, 1046−1055

Supporting information - Utilizing lubricant loss from Omniphobic coatings as a multi-functional delivery mechanism

CORRESPONDING AUTHOR

Callum. A.C. Stewart - Ming Wai Lau Centre for Reparative Medicine, Karolinska Institutet, 15W Science Park W Ave, Hong Kong. Email: callum.stewart@ki.se

AUTHORS

Babak Mehrjou - Department of Materials Science and Engineering, Department of Physics and Department of Biomedical Engineering, City University of Hong Kong, Hong Kong

Hui Huang - Ming Wai Lau Centre for Reparative Medicine, Karolinska Institutet, 15W Science Park W Ave, Hong Kong

Yunxin Long - Ming Wai Lau Centre for Reparative Medicine, Karolinska Institutet, 15W Science Park W Ave, Hong Kong

Kyler Chow - Ming Wai Lau Centre for Reparative Medicine, Karolinska Institutet, 15W Science Park W Ave, Hong Kong

Tsz Wai Kok - Developmental and Regenerative Biology TRP, School of Biomedical Sciences, Faculty of Medicine, The Chinese University of Hong Kong

Paul K. Chu - Department of Materials Science and Engineering, Department of Physics and Department of Biomedical Engineering, City University of Hong Kong, Hong Kong

Linxian Li - Ming Wai Lau Centre for Reparative Medicine, Karolinska Institutet, 15W Science Park W Ave, Hong Kong

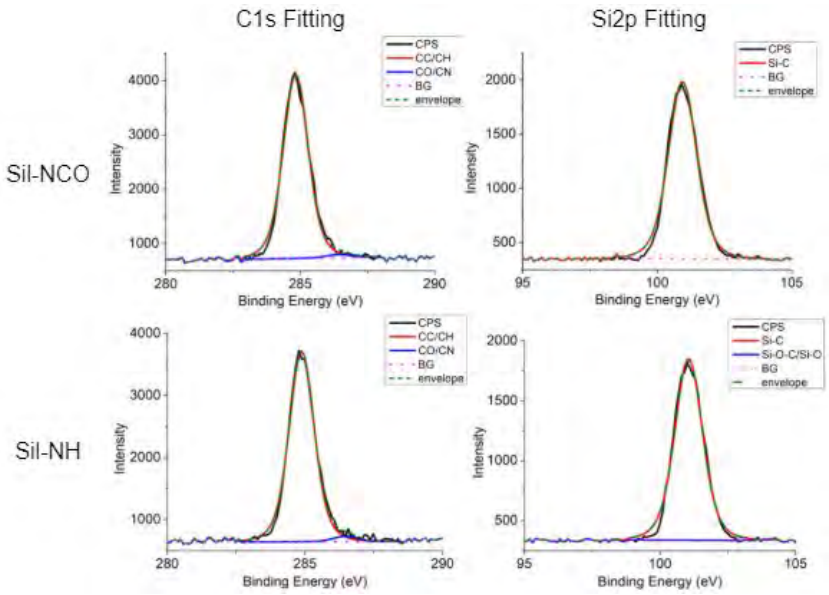

Figure S1: The Sil_NCO spectrum elemental compositions (at%): C= 47.18%, N= 0.61%, O= 19.55%, Si = 32.67%. The Sil-NH spectrum elemental composition (at%): C = 46.8%, N=0%, O= 18.28%, Si= 34.92%. The C1s peaks of both precursors were highly monodispersed around the 284.8eV region associated with the C-C/C-H fitting. Likewise, the Si2p spectra were strongly monodispersed around 101 eV which is fitted to the Si-C. These elemental

compositions and peak fitting are consistent with the chemical structures for the corresponding reagents, a methyl Si-O polymer backbone with functional terminals consisting of amines or isocyano groups attached to cyclic carbons. The nature of the fittings provides a clear distinction between the initial precursors and the final gel matrix.

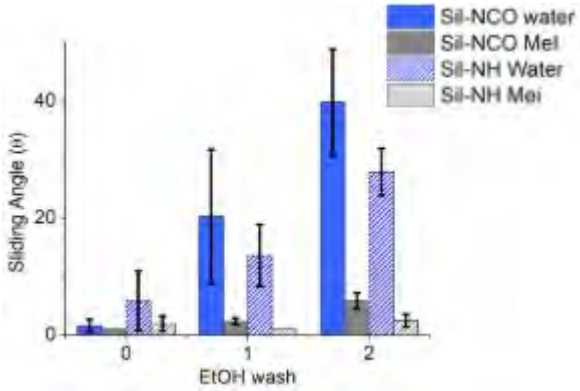

Figure S2. Sliding and contact angles for the Silmer NCO Di-50 (Sil-NCO) and Silmer NH C50 (Sil-NH) deposited on glass substrates. The Diiodomethane (MeI) sliding angles remained low on both components due to the repellent dispersive/ non-polar interactions between the Silicone backbones and the MeI. The water sliding angles demonstrated significant increases beyond the 1:1 ratio Siligel equivalent. While a small degree of self-interaction may be present due to the decomposition of NCO into NH_2, there is a strong indication that the enduring wetting properties of the Siligel is due to the formation of a gel matrix and release of entrapped Silicone oil.

Figure S3. Contact and sliding measurements of MeI and Water on the 0wt% and 5wt% Ag NP Siligel coatings. Images show typical CA and SAs at the initial 0x wash and final 5x wash in pure EtOH.

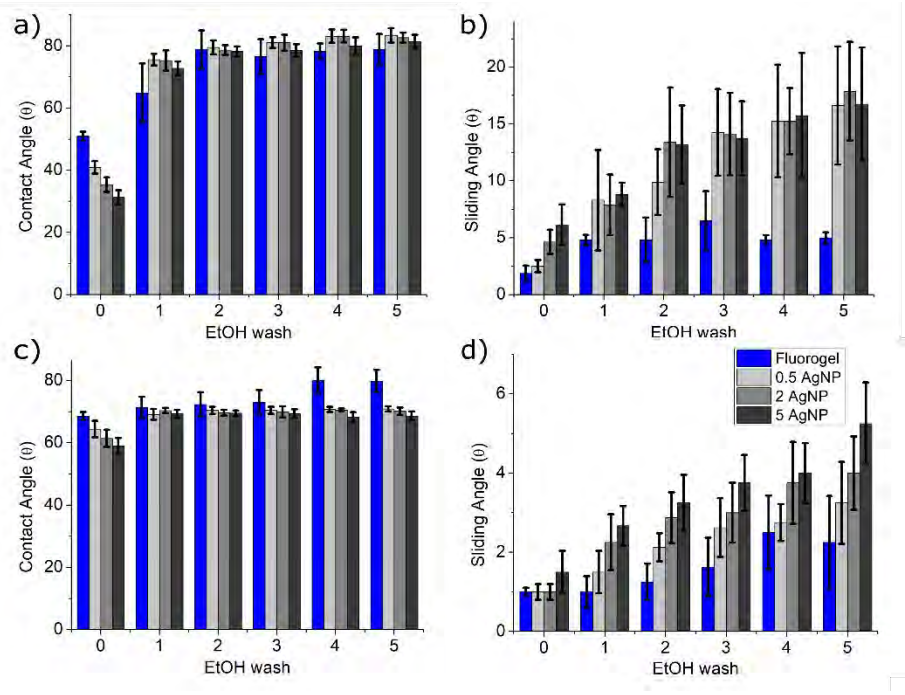

Figure S4: The wetting measurements for Fluorogels at increasing Ag NP wt%; **a)** water contact angle, **b)** water sliding angle, **c)** MeI contact angle, and **d)** MeI sliding angle.

Table S1. Sliding distance and time for foodstuffs on untreated, Fluorogel, and Siligel surfaces.

Food	**Inclination (°)**	**Coating**	**Time (Sec)**	**distance (cm)**
Jam	25	Uncoated	110	0
		Fluorogel	45	3
		Siligel	50	7
Honey	25	Uncoated	55	7

		Fluorogel	50	6.5
		Siligel	23	7
ketchup	25	Uncoated	120	3
		Fluorogel	140	7
		Siligel	60	6
yogurt	39	Uncoated	110	3
		Fluorogel	90	7
		Siligel	40	7

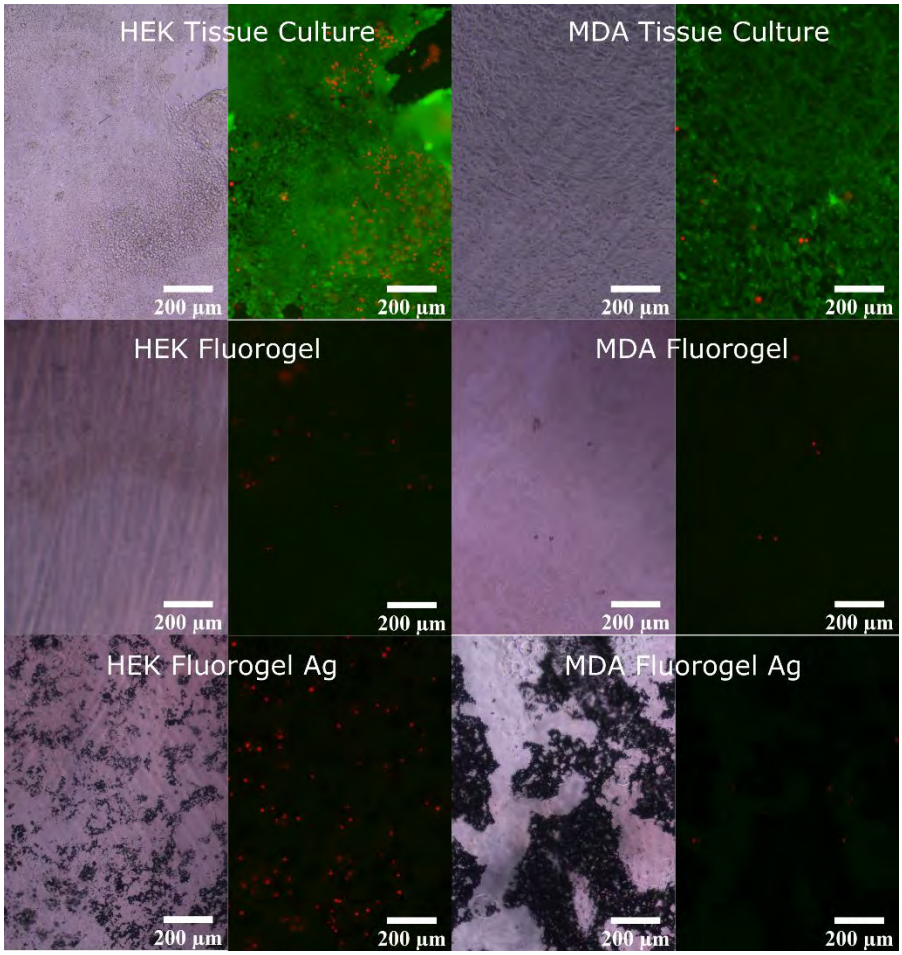

Figure S5: Contrast and Live/ Dead fluorescence microscopy images of the MDA-MB and HEK permanent cell lines at 10x magnification after 7 days on TCP and Fluorogel coatings at 0 wt% and 2wt% AgNP.